

# Triaxial projected shell model study of $\gamma$ -bands in atomic nuclei

S. Jehangir<sup>2</sup>, G.H. Bhat<sup>1,3,4</sup>, J.A. Sheikh<sup>4</sup>, S. Frauendorf<sup>5</sup>, W. Li<sup>5</sup>, and R. Palit<sup>2</sup>

<sup>1</sup> Department of Physics, S.P. College, Srinagar, Jammu and Kashmir, 190001, India

<sup>2</sup> Department of Nuclear and Atomic Physics, Tata Institute of Fundamental Research, Mumbai - 400005, India

<sup>3</sup> Cluster University Srinagar, Jammu and Kashmir, Srinagar, Goji Bagh, 190008, India

<sup>4</sup> Department of Physics, University of Kashmir, Hazratbal, Srinagar, 190006, India and

<sup>5</sup> Physics Department, University of Notre Dame, Notre Dame, Indiana 46556, USA

(Dated: September 10, 2020)

A systematic study of  $\gamma$ -bands observed in atomic nuclei is performed using the triaxial projected shell model (TPSM) approach. The staggering phase between the even and odd spin members of the  $\gamma$ -band for most the nuclei investigated in the present work is found to have even-I-below-odd-I, which in the framework of the collective model is considered as a signature of  $\gamma$ -softness. It is observed that out of twenty-three systems studied, only four nuclei, namely, <sup>76</sup>Ge, <sup>112</sup>Ru, <sup>170</sup>Er and <sup>232</sup>Th depict staggering phase with odd-I-below-even-I, which is regarded as an indication of the static  $\gamma$ -deformation in the collective model picture. The inclusion of the quasiparticle excitations in the framework of configuration mixing is shown to reverse the staggering phase from odd-I-down to the even-I-down for all the studied nuclei, except for the aforementioned four nuclei. Furthermore, by fitting a collective Bohr Hamiltonian to the TPSM energies, the differences between the two models are delineated through a comparison of the transition probabilities.

PACS numbers: 21.60.Cs, 21.10.Hw, 21.10.Ky, 27.50.+e

## I. INTRODUCTION

Spontaneous breaking of rotational symmetry that leads to the deformation of a quantum system in the intrinsic frame, has played a pivotal role to unravel the underlying shapes and structures of atomic nuclei [1]. The properties of deformed nuclei are elucidated by considering the ellipsoidal shape, which is conveniently parameterized in terms of axial and non-axial deformation parameters of  $\beta$  and  $\gamma$ . The majority of the deformed nuclei are axially-symmetric ( $\gamma = 0$ ) with angular-momentum projection along the symmetry axis,  $K$ , a conserved quantum number with the electromagnetic transition probabilities obeying the selection rules based on this quantum number [2, 3]. There are also regions in the nuclear periodic table, referred to as transitional, where the axial symmetry is broken and the non-axial degree of freedom plays an essential role to determine the properties of these nuclei.

In the traditional picture, atomic nuclei may have either a localized minimum or a flat potential energy surface along the  $\gamma$ - degree of freedom, corresponding to  $\gamma$ -rigid and  $\gamma$ -soft nuclei, respectively [4–7]. How to distinguish between the two kinds of shapes from the observable properties has been of considerable interest in nuclear physics for more than sixty years. To address the question properly one needs to complement the potential by inertial parameters to estimate the spread of the wave around the minimum, which is accomplished in various ways. The phenomenological Bohr Hamiltonian [3, 8] assumes irrotational-flow inertia and has the two limiting cases. The one limiting case, referred to as the Davydov-Filippov model [9] describes a rigid triaxial shape, which corresponds to a deep potential minimum with respect to both  $\beta$  and  $\gamma$ . The second case, called as Wilets-Jean model [10], describes the completely  $\gamma$ -soft limit and corresponds to a deep potential minimum with respect to  $\beta$  and no  $\gamma$ - dependence. Both limiting cases give rise to similar excitation spectrum for the ground-state band [9, 10]. This holds as well

for intermediate cases studied in Ref. [8], where the author found that the average energy of the  $\gamma$ - band is insensitive to the rigidity of the  $\gamma$ - degree of freedom. It is, therefore, impossible to distinguish between soft- and rigid- triaxiality from rich data of this kind that is available for most of the nuclei.

The energy staggering in the  $\gamma$ -band, on the other hand, is sensitive to the softness of the  $\gamma$ -degree of freedom [4]. For  $\gamma$ -soft nuclei (Wilets-Jean limit), the energies of the  $\gamma$ -band are bunched as  $(2^+), (3^+, 4^+), (5^+, 6^+), \dots$ , which we refer to as "even-I-down", and for  $\gamma$ -rigid nuclei (Davydov-Filippov limit), the energy levels of the  $\gamma$ -band are arranged as  $(2^+, 3^+), (4^+, 5^+), (6^+, 7^+), \dots$ , which we shall call as "odd-I-down". This implies that the sequence of energy levels of the  $\gamma$ -band shall lead to opposite phase of the staggering parameter, defined below, in the two cases. More detailed discussions on the subject can be found, e. g., in Refs. [8, 11]. The microscopic versions of the Bohr Hamiltonian, pioneered in Ref. [6] (for a review of recent work, see [11]), are based on a potential and inertial parameters, derived by applying the adiabatic approximation to the time-dependent mean-field theory. Although not explicitly studied, the same correlation between  $\gamma$ -softness and staggering of the  $\gamma$ - band levels is found. A similar pattern concerning the rigidity of the  $\gamma$ - degree of freedom is obtained in the framework of the interacting boson model [12, 13]. The correlation between  $\gamma$ - rigidity and staggering is discussed in detail in Ref. [11]. It has to be underlined at this point that correlation appears in models that assume an adiabatic separation between the collective quadrupole degrees of freedom and the quasiparticle excitations.

The present work investigates the  $\gamma$ -band staggering in even-even nuclei using the microscopic triaxial projected shell model (TPSM) approach [14], which is based on assumptions that are different from above discussed collective models. The TPSM assumes a *fixed* triaxial deformation, and

the coupling to the quasiparticle excitations is taken into account using the configuration mixing. The present study has been performed for all the nuclei in the periodic table for which  $\gamma$ -bands are observed up to high angular momentum, for both even- and odd-spin members. It is demonstrated that angular-momentum projection from the intrinsic triaxial vacuum gives rise to odd- $I$ -down  $\gamma$ -band staggering, which is expected because the angular momentum components projected from 0-quasiparticle state establish a microscopic version of the Davydov-Filippov model of rigid- $\gamma$  motion. However, it is shown that inclusion of quasiparticle excitations transforms the odd- $I$ -down staggering into even- $I$ -down staggering, associated with  $\gamma$ -softness, for all even-even nuclei studied in the present work, except for four nuclei of  $^{76}\text{Ge}$ ,  $^{112}\text{Ru}$ ,  $^{170}\text{Er}$  and  $^{232}\text{Th}$ .

We have also investigated  $\gamma$ -bands using the Bohr Hamiltonian by adjusting its parameters to reproduce the TPSM transition energies. It is demonstrated that the  $\gamma$ -band staggering obtained in this model is quite similar to that of the TPSM approach. For  $^{104,106,108}\text{Mo}$  and  $^{108,110,112}\text{Ru}$ , we also evaluated  $B(E2)$  values for intra-band and inter-band transitions in the two approaches. In comparison to the TPSM results, a large reduction of the  $B(E2, I_\gamma \rightarrow (I-1)_{\text{ground}}$  for  $I > 3$  and of the  $B(E2, I_\gamma \rightarrow (I-2)_{\text{ground}}$  for  $I > 4$  values is observed in the collective model.

The manuscript is organized in the following manner. Section II contains brief description of TPSM approach, more details on the model can be found in our earlier publications [15–17]. The results obtained from the TPSM calculations on the nature of  $\gamma$ -bands are analyzed in Section III. A. In section III. B, the TPSM transition probabilities are compared with the ones obtained using the Bohr Hamiltonian and finally section IV contains some concluding remarks.

## II. OUTLINE OF THE TRIAXIAL PROJECTED SHELL MODEL APPROACH

For even-even systems, the TPSM basis space is composed of projected 0-qp state (or qp-vacuum  $|\Phi\rangle$ ), 2-proton, 2-neutron, and 4-qp configurations, i.e.,

$$\begin{aligned} & \hat{P}_{MK}^I |\Phi\rangle; \\ & \hat{P}_{MK}^I a_{p_1}^\dagger a_{p_2}^\dagger |\Phi\rangle; \\ & \hat{P}_{MK}^I a_{n_1}^\dagger a_{n_2}^\dagger |\Phi\rangle; \\ & \hat{P}_{MK}^I a_{p_1}^\dagger a_{p_2}^\dagger a_{n_1}^\dagger a_{n_2}^\dagger |\Phi\rangle, \end{aligned} \quad (1)$$

where the three-dimensional angular-momentum operator [18] is given by

$$\hat{P}_{MK}^I = \frac{2I+1}{8\pi^2} \int d\Omega D_{MK}^I(\Omega) \hat{R}(\Omega), \quad (2)$$

with the rotation operator

$$\hat{R}(\Omega) = e^{-i\alpha\hat{J}_z} e^{-i\beta\hat{J}_y} e^{-i\gamma\hat{J}_z}. \quad (3)$$

Here, " $\Omega$ " represents a set of Euler angles ( $\alpha, \gamma = [0, 2\pi]$ ,  $\beta = [0, \pi]$ ) and the  $\hat{J}$ 's are angular-momentum operators. The

triaxial vacuum configuration is a superposition of  $K$ -configurations and it can be easily shown that only even- $K$  values are permitted due to symmetry requirement [19]. The projected bands from the vacuum state with  $K=0, 2$  and 4 in the  $D$ -matrix result into ground-,  $\gamma$ - and  $\gamma\gamma$ -bands, respectively. For two-quasiparticle states, both even- and odd- $K$  values are permitted, depending on the nature of the quasiparticles. For a two quasiparticle configuration formed from normal and time-reversed states, only even- $K$  are permitted. However, with both the states either normal or time-reversed, odd- $K$  values are allowed from symmetry considerations.

The projected basis constructed above are then employed to diagonalize the shell model Hamiltonian. As in the earlier TPSM calculations, we use the pairing plus quadrupole-quadrupole Hamiltonian:

$$\hat{H} = \hat{H}_0 - \frac{1}{2}\chi \sum_{\mu} \hat{Q}_{\mu}^{\dagger} \hat{Q}_{\mu} - G_M \hat{P}^{\dagger} \hat{P} - G_Q \sum_{\mu} \hat{P}_{\mu}^{\dagger} \hat{P}_{\mu}, \quad (4)$$

with the last term in (4) being the quadrupole-pairing force. The corresponding triaxial Nilsson mean-field Hamiltonian, which is obtained by using the Hartree-Fock-Bogoliubov (HFB) approximation, is given by

$$\hat{H}_N = \hat{H}_0 - \frac{2}{3}\hbar\omega \left\{ \varepsilon \hat{Q}_0 + \varepsilon' \frac{\hat{Q}_{+2} + \hat{Q}_{-2}}{\sqrt{2}} \right\}. \quad (5)$$

Here  $\hat{H}_0$  is the spherical single-particle Hamiltonian, which contains a proper spin-orbit force [20]. The interaction strengths are taken as follows: The  $QQ$ -force strength  $\chi$  is adjusted such that the physical quadrupole deformation  $\varepsilon$  is obtained as a result of the self-consistent mean-field HFB calculations. The monopole pairing strength  $G_M$  is of the standard form

$$G_M = (G_1 \mp G_2 \frac{N-Z}{A}) \frac{1}{A} \text{ (MeV)}, \quad (6)$$

where  $-(+)$  is neutron (proton). In the present calculation, we use  $G_1$  and  $G_2$ , which approximately reproduce the observed odd-even mass difference in the region under investigation. This choice of  $G_M$  is appropriate for the single-particle space employed in the model, where three major shells are used for each type of nucleons. The quadrupole pairing strength  $G_Q$  is assumed to be proportional to  $G_M$ , and the proportionality constant being fixed as 0.16. These interaction strengths are consistent with those used in our earlier studies [15–17].

The projection formalism outlined above can be transformed into a diagonalization problem following the Hill-Wheeler approach, i.e.,

$$\begin{aligned} & \sum_{K', \kappa'} \langle \Phi_{\kappa} | \hat{H} \hat{P}_{KK'}^I | \Phi_{\kappa'} \rangle \\ & - E_I \langle \Phi_{\kappa} | \hat{P}_{KK'}^I | \Phi_{\kappa'} \rangle f_{K'\kappa'}^I = 0, \end{aligned} \quad (7)$$

where  $f_{K\kappa}^I$  are the variational coefficients. The projected wavefunction in terms of these coefficients can be written as

$$\Psi_{IM} = \sum_{K, \kappa} f_{K\kappa}^I \hat{P}_{MK}^I | \Phi_{\kappa} \rangle. \quad (8)$$

In the above equations, the symbol  $\kappa$  represents the basis states of Eq. (1). These wavefunctions are used to calculate the electromagnetic transition probabilities. The reduced electric quadrupole transition probability  $B(E2)$  from an initial state  $(\sigma_i, I_i)$  to a final state  $(\sigma_f, I_f)$  is given by [21]

$$B(E2, I_i \rightarrow I_f) = \frac{e^2}{2I_i + 1} |\langle \sigma_f, I_f | \hat{Q}_2 | \sigma_i, I_i \rangle|^2. \quad (9)$$

As in our earlier publications [15, 16, 22–24], we have used the effective charges of 1.5e for protons and 0.5e for neutrons. The effective charges are employed instead of the bare charges as core is used in the TPSM and valance particles occupy only three major oscillator shells. The reduced magnetic dipole transition probability  $B(M1)$  is computed through

$$B(M1, I_i \rightarrow I_f) = \frac{\mu_N^2}{2I_i + 1} |\langle \sigma_f, I_f | \hat{\mathcal{M}}_1 | \sigma_i, I_i \rangle|^2, \quad (10)$$

where the magnetic dipole operator is defined as

$$\hat{\mathcal{M}}_1^\tau = g_l^\tau \hat{j}^\tau + (g_s^\tau - g_l^\tau) \hat{s}^\tau. \quad (11)$$

Here,  $\tau$  is either  $\nu$  or  $\pi$ , and  $g_l$  and  $g_s$  are the orbital and the spin gyromagnetic factors, respectively. In the calculations we use for  $g_l$  the free values and for  $g_s$  the free values damped by a 0.85 factor, i.e.,

$$\begin{aligned} g_l^\pi &= 1, & g_l^\nu &= 0, \\ g_s^\pi &= 5.586 \times 0.85, \\ g_s^\nu &= -3.826 \times 0.85. \end{aligned} \quad (12)$$

The reduced matrix element of an operator  $\hat{\mathcal{O}}$  ( $\hat{\mathcal{O}}$  is either  $\hat{Q}$  or  $\hat{\mathcal{M}}$ ) can be expressed as

$$\begin{aligned} & \langle \sigma_f, I_f | \hat{\mathcal{O}}_L | \sigma_i, I_i \rangle \\ &= \sum_{\kappa_i, \kappa_f} a_{\kappa_i}^{\sigma_i} a_{\kappa_f}^{\sigma_f} \sum_{M_i, M_f, M} (-)^{I_f - M_f} \\ & \times \begin{pmatrix} I_f & L & I_i \\ -M_f & M & M_i \end{pmatrix} \\ & \times \langle \Phi_{\kappa_f} | \hat{P}_{\kappa_f, M_f}^{I_f} \hat{\mathcal{O}}_{LM} \hat{P}_{\kappa_i, M_i}^{I_i} | \Phi_{\kappa_i} \rangle \\ &= 2 \sum_{\kappa_i, \kappa_f} a_{\kappa_i}^{\sigma_i} a_{\kappa_f}^{\sigma_f} \sum_{M', M''} (-)^{I_f - K_{\kappa_f}} (2I_f + 1)^{-1} \\ & \times \begin{pmatrix} I_f & L & I_i \\ -K_{\kappa_f} & M' & M'' \end{pmatrix} \int d\Omega D_{M'' K_{\kappa_i}}^{I_i}(\Omega) \\ & \times \langle \Phi_{\kappa_f} | \hat{\mathcal{O}}_{LM'} \hat{R}(\Omega) | \Phi_{\kappa_i} \rangle. \end{aligned} \quad (13)$$

In the above expression, the symbol  $\begin{pmatrix} \phantom{a} \\ \phantom{a} \\ \phantom{a} \end{pmatrix}$  denotes a 3j-coefficient.

### III. RESULTS AND DISCUSSIONS

It has been demonstrated in several previous studies [15–17, 22–26] that TPSM approach reproduces the high-spin properties of deformed and transitional nuclei quite accurately. As an illustrative example, TPSM calculated energies of the yrast-,  $\gamma$ - and  $\gamma\gamma$ - bands of  $^{158}\text{Dy}$  nucleus are

TABLE I. Parameters used in calculations

Nuclei	Configuration Space	$G_1$	$G_2$
$^{154,156}\text{Gd}$	$N_\nu = 4, 5, 6$	21.24	13.86
$^{156,158,160,162}\text{Dy}$	$N_\pi = 3, 4, 5$		
$^{164,166,168,170}\text{Er}$			
$^{180}\text{Hf}$			
$^{232}\text{Th}, ^{238}\text{U}$	$N_\nu = 5, 6, 7$	16.80	12.80
	$N_\pi = 4, 5, 6$		
$^{104,106,108}\text{Mo}$	$N_\nu = 3, 4, 5$	22.68	16.22
$^{108,110,112,114}\text{Ru}$	$N_\pi = 2, 3, 4$		
$^{76}\text{Ge}, ^{76,78}\text{Se}$	$N_\nu = 2, 3, 4$	20.82	13.58
	$N_\pi = 2, 3, 4$		

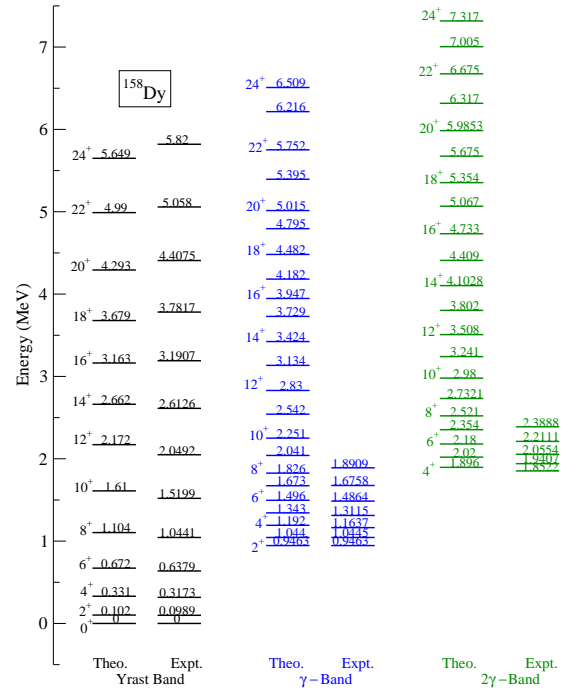


FIG. 1. (Color online) Comparison of the TPSM energies after configuration mixing with the available experimental data for  $^{158}\text{Dy}$ . Data is taken from [30, 31].

displayed in Fig. 1 along with the known experimental energies. It is evident from the results that TPSM approach reproduces the experimental data quite reasonably. In particular, it is noted that predicted  $\gamma$ -band transition energies agree quite well with the known experimental values. In the following, we now address the main topic of the manuscript : to investigate the correlation between the nature of the  $\gamma$ - deformation and the staggering phase of the  $\gamma$ -bands.

TABLE II. Axial and triaxial quadrupole deformation parameters  $\varepsilon$  and  $\varepsilon'$  employed in the TPSM calculation. Axial deformations are taken from [32] and nonaxial deformations are chosen in such a way that band heads of the  $\gamma$ -bands are reproduced. In this table, we also provide the ratios,  $\frac{E(2_2^+)}{E(2_1^+)}$ , using both experimental and TPSM energies.

	$^{154}\text{Gd}$	$^{156}\text{Gd}$	$^{156}\text{Dy}$	$^{158}\text{Dy}$	$^{160}\text{Dy}$	$^{162}\text{Dy}$	$^{164}\text{Er}$	$^{166}\text{Er}$	$^{168}\text{Er}$	$^{170}\text{Er}$	$^{180}\text{Hf}$	$^{232}\text{Th}$	$^{238}\text{U}$	$^{104}\text{Mo}$	$^{106}\text{Mo}$	$^{108}\text{Mo}$	$^{108}\text{Ru}$	$^{110}\text{Ru}$	$^{112}\text{Ru}$	$^{114}\text{Ru}$	$^{76}\text{Ge}$	$^{76}\text{Se}$	$^{78}\text{Se}$
$\varepsilon$	0.300	0.341	0.278	0.260	0.270	0.280	0.317	0.325	0.321	0.319	0.195	0.248	0.210	0.320	0.310	0.294	0.280	0.290	0.289	0.250	0.200	0.260	0.256
$\varepsilon'$	0.100	0.100	0.105	0.110	0.110	0.120	0.120	0.126	0.130	0.110	0.090	0.085	0.085	0.130	0.110	0.140	0.150	0.130	0.080	0.080	0.160	0.155	0.150
$\gamma$	18.4	16.3	20.7	22.9	22.1	23.2	20.7	21.2	22.1	19.0	24.7	18.9	22.0	22.1	19.5	25.4	28.2	27.3	24.2	17.7	38.6	30.8	30.2
$\left[\frac{E(2_2^+)}{E(2_1^+)}\right]_{\text{Expt.}}$	8.0	12.9	6.5	9.6	11.1	9.7	10.4	9.7	10.3	11.8	12.9	15.9	21.2	4.2	4.1	3.0	2.9	2.5	2.2	2.1	1.9	2.2	2.1
$\left[\frac{E(2_2^+)}{E(2_1^+)}\right]_{\text{TPSM}}$	10.6	12.1	9.7	9.5	12.9	11.9	9.4	10.5	11.7	13.4	15.4	15.3	20.7	5.3	5.1	3.6	3.5	3.4	3.2	2.4	2.1	2.2	2.2

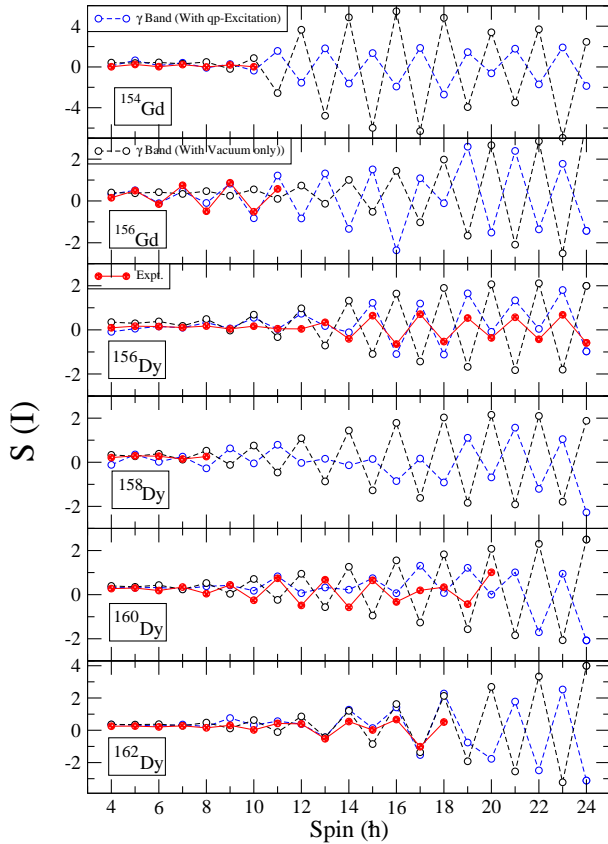


FIG. 2. (Color online) Comparison of observed and TPSM calculated staggering parameter Eq. (14) for the  $\gamma$ -band with and without quasiparticle excitations for  $^{156,158}\text{Gd}$  and  $^{156,158,160,162}\text{Dy}$  nuclei. Data is taken from Refs. [33–39].

### A. Staggering of the $\gamma$ -bands

A systematic investigation of the  $\gamma$ -bands using TPSM framework has been performed for even-even nuclei listed in Table I. For the chosen twenty-three nuclei,  $\gamma$ -bands for both even- and odd-spin signatures are observed up to quite high-spin and it is possible to investigate the odd-even staggering

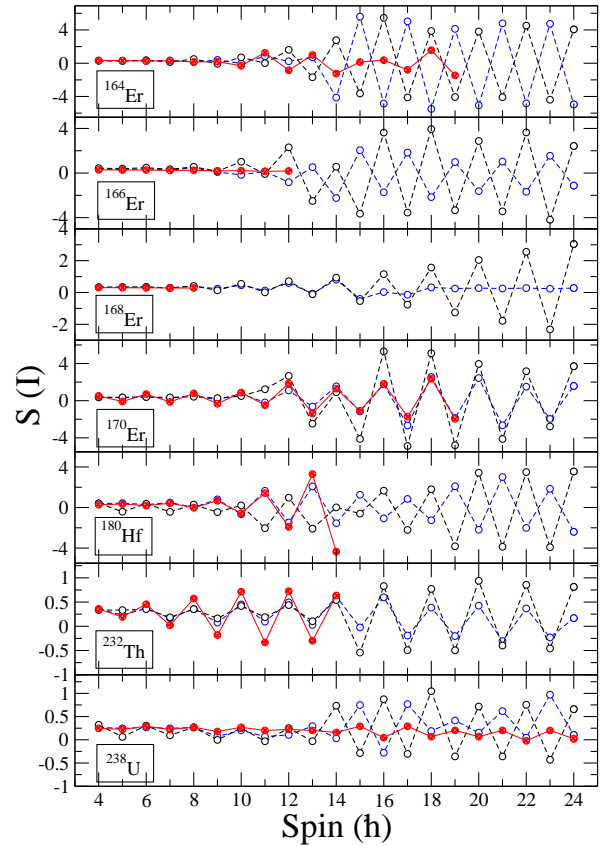


FIG. 3. (Color online) Comparison of observed and TPSM calculated staggering parameter Eq. (14) for the  $\gamma$ -band with and without quasiparticle excitations for  $^{164,166,168,170}\text{Er}$ ,  $^{180}\text{Hf}$ ,  $^{232}\text{Th}$  and  $^{238}\text{U}$  nuclei. Data is taken from Refs. [40–45].

as a function of the spin. This table also provides the information on the configuration space and pairing strengths used in different regions. Deformation parameters of  $\varepsilon$  and  $\varepsilon'$  employed in the TPSM calculations are provided in Table II. The axial deformation parameter,  $\varepsilon$  is either fixed such that the observed quadrupole moment of the first excited state is reproduced or from other theoretical studies. The triaxiality pa-

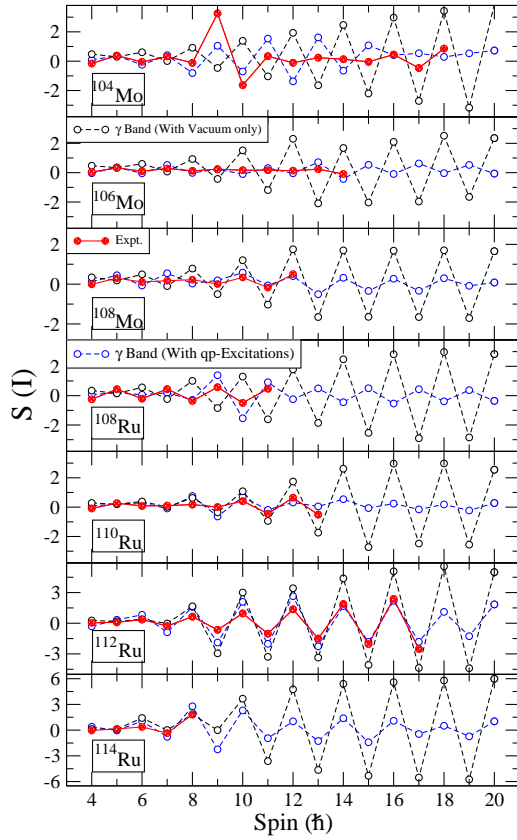


FIG. 4. (Color online) Comparison of observed and TPSM calculated staggering parameter Eq. (14) for the  $\gamma$ -band with and without quasiparticle excitations for  $^{104,106,108}\text{Mo}$  and  $^{108,110,112,114}\text{Ru}$  nuclei. Data is taken from Refs. [46–50].

parameter,  $\varepsilon'$  is determined so that the band-head of the  $\gamma$ -band is reproduced, a prescription adopted in most of our earlier works [15, 16, 24–26]. There are other ways of choosing this parameter. One can use the tidal wave version of the cranking model [27], which has been applied to  $^{156}\text{Dy}$  [25]. A related approach is to look for the potential energy minimum with respect to  $\varepsilon'$  as a generator coordinate. It has been shown in our earlier work [15] that this leads to a similar nonaxial deformation value as that deduced through fixing the band-head energy of the  $\gamma$ -band.

As alluded to in the introduction, in the framework of collective models with quadrupole degrees freedom, the staggering parameter, defined as

$$S(I) = \frac{[E(I) - E(I-1)] - [E(I-1) - E(I-2)]}{E(2_1^+)}, \quad (14)$$

is strongly correlated with the rigidity of the triaxial shape : the odd-I-down pattern indicates the concentration of the collective wave function around a finite  $\gamma$ -value (static triaxiality), whereas the even-I-down pattern points to a spread of the

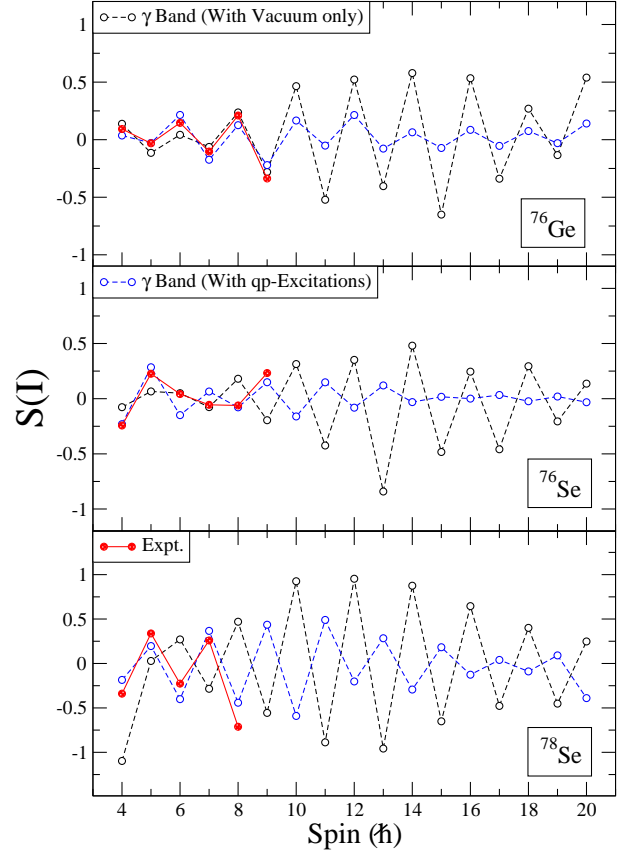


FIG. 5. (Color online) Comparison of observed and TPSM calculated staggering parameter Eq. (14) for the  $\gamma$ -bands in  $^{76}\text{Ge}$  and  $^{76,78}\text{Se}$  nuclei. Data is taken from Refs. ([28, 51, 52])

wave function over the whole range of  $\gamma$  (dynamic triaxiality). The correlation is reviewed in Ref. [11], where the relevant literature is cited.

In Figs. 2 - 4, the TPSM results for  $S(I)$  are plotted for twenty nuclei in different regions of the nuclear chart, which have been selected as  $\gamma$ -bands, both for even- and odd-spin signatures, have been observed up to quite high spin. In Figs. 2 and 3 the results of  $S(I)$  are depicted for  $^{154,156}\text{Gd}$ ,  $^{156,158,160,162}\text{Dy}$ ,  $^{164,166,168,170}\text{Er}$ ,  $^{180}\text{Hf}$ ,  $^{232}\text{Th}$  and  $^{238}\text{U}$ . The figures compare the TPSM calculations that are obtained from the projection of zero-quasiparticle state only with the full TPSM calculations that include all the projected quasiparticle configurations, listed in Eq. 1. The restricted TPSM calculations represent a microscopic version of the Davydov-Filippov model : the different  $K$  components for given  $I$  are projected from one and the same intrinsic zero-quasiparticle state and the resulting matrix of the TPSM Hamiltonian diagonalized. Therefore, it is expected that  $S(I)$  depicts the odd-I-down pattern of the rigid rotor, which is borne out of the calculations.

However, Figs. 2 and 3 demonstrate that the phase of the staggering changes to even-I-down when the quasiparticle ex-

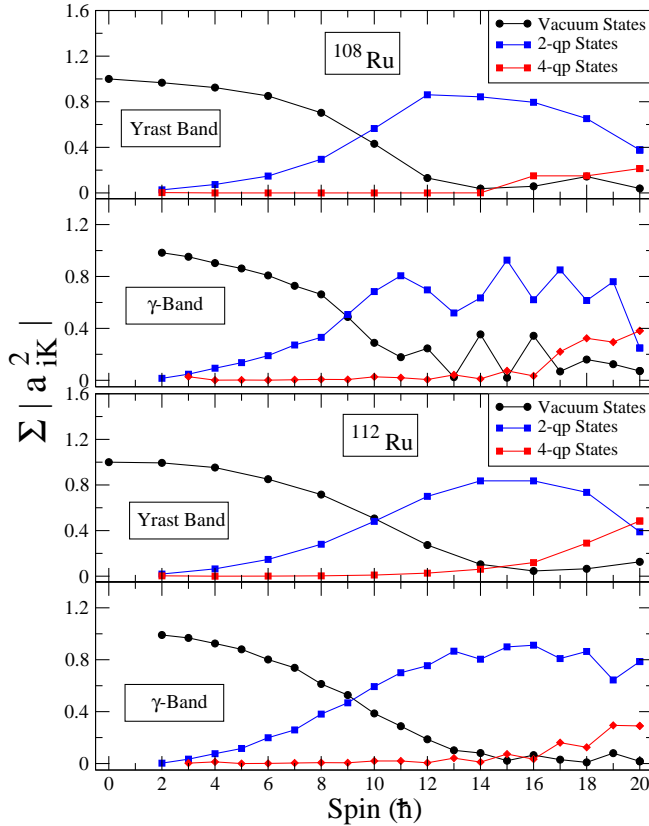


FIG. 6. (Color online) Probability of various projected  $K$ -configurations in the wavefunctions of the band structures after diagonalization are plotted for the  $^{108,112}\text{Ru}$  isotopes.

citation in the configuration mixing framework are taken into account for all the nuclei, except for  $^{170}\text{Er}$  and  $^{232}\text{Th}$ . For the case of  $^{162}\text{Dy}$ , the staggering phase in the spin regime from  $I=12$  to  $18$  is same with and without quasiparticle excitations, however, for higher spin states the phase reverses. The TPSM values correlate well with the available experimental staggering pattern, which are also plotted in the figures. The only exceptional case is  $^{238}\text{U}$ , for which the difference between the calculated and the experimental staggering appears somewhat larger. However, it may be noted that the magnitude of the staggering as compared to other nuclei in Fig. 3 is quite small for this system.

The staggering parameters for Mo- and Ru-isotopes are depicted in Fig. 4. For  $^{104,106}\text{Mo}$ , the phase of staggering changes when the quasiparticle excitations are taken into account. For  $^{108}\text{Mo}$ , inclusion of the quasiparticle excitation reverses the staggering phase up to  $I=8$ , but above this spin the staggering remains odd- $I$ -down. In the case of  $^{108}\text{Ru}$ , inclusion of the quasiparticle excitations reverses the staggering phase. For  $^{110}\text{Ru}$ , the magnitude of the staggering phase is small for low spin and becomes odd- $I$ -down for high spin. The

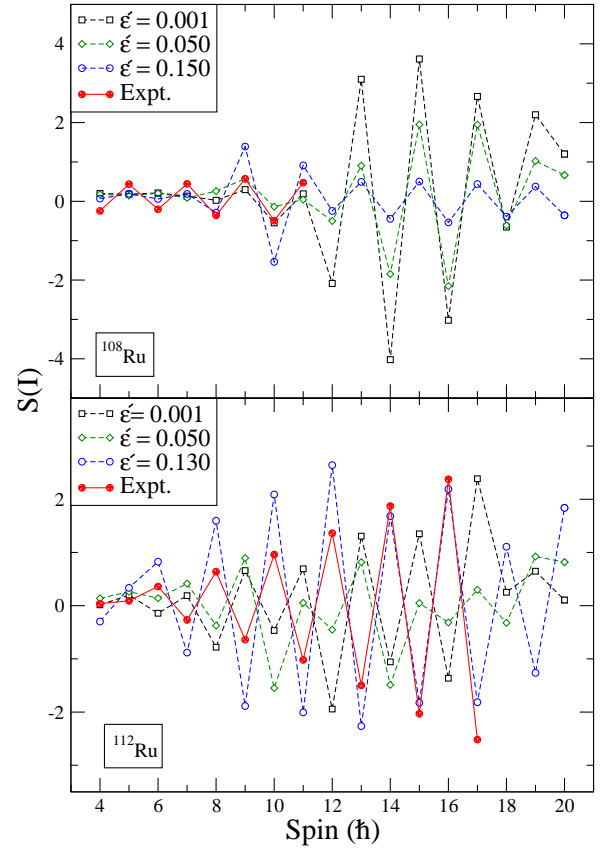


FIG. 7. (Color online) Comparison of observed and TPSM calculated staggering parameter Eq. (14) for the  $\gamma$ -bands in  $^{108,112}\text{Ru}$  isotopes for the different values of  $\epsilon'$ .

nuclide  $^{112}\text{Ru}$  shows well pronounced odd- $I$ -down staggering, which is not modified when including the quasiparticle excitations. The case of  $^{114}\text{Ru}$  is similar to  $^{110}\text{Ru}$ , only the amplitude of the staggering is smaller. As seen in Fig. 4, the TPSM results correlate impressively well with the experimental  $S(I)$  values. It is noted that in  $^{108}\text{Mo}$  and  $^{110}\text{Ru}$ , the staggering changes from weak even- $I$ -up to odd- $I$ -down around  $I=8$ . In  $^{112,114}\text{Ru}$ , the odd- $I$ -down staggering sets-in at  $I=6$ , which is reproduced by the TPSM results.

In the mass 80 region,  $\gamma$ -bands have also been observed in some nuclei up to high spin. In Ref. [15], the isotopes  $^{76-82}\text{Se}$  and  $^{70-80}\text{Ge}$  have been investigated in the framework TPSM approach. The staggering parameter,  $S(I)$  has been found with even- $I$ -down for all nuclides except  $^{76}\text{Ge}$ , which has odd- $I$ -down. The TPSM results for  $^{76}\text{Ge}$  and  $^{76,78}\text{Se}$  agree well with the experimental  $S(I)$  as shown in Fig. 5. Based on the odd- $I$ -down pattern [28] and  $E2$  reduced transition matrix elements measured in Coulomb excitation experiment [29],  $^{76}\text{Ge}$  has been featured as a rare example of a  $\gamma$ -rigid nucleus.

The fact that the TPSM results with quasiparticle excitations account for the experimental staggering parameter is sur-

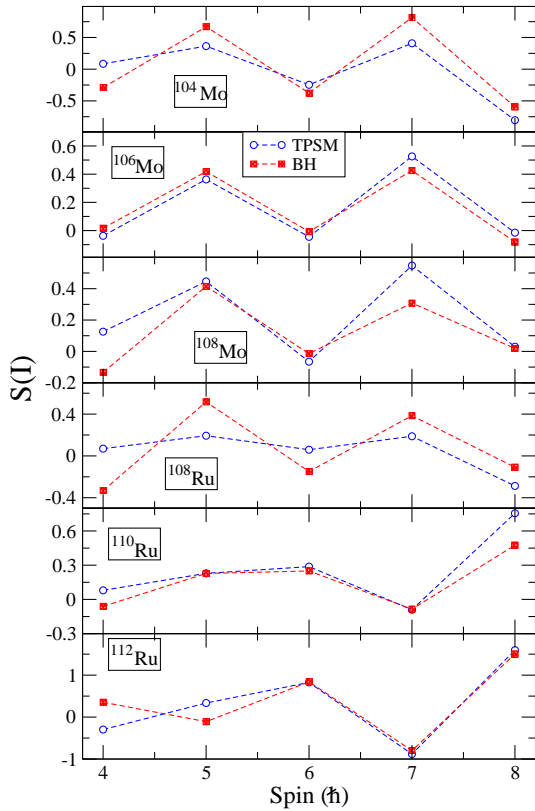


FIG. 8. (Color online) Comparison of the staggering parameter calculated by means of the TPSM (blue circles) and the BH (red squares).

prising, because the even- $I$ -down staggering is associated with  $\gamma$  softness (Wilet-Jean limit) in the context of the collective model. The TPSM assumes a fixed value of  $\gamma$  and restricting the configuration space to the  $K$ -projections from the zero quasiparticle state only, always results in odd- $I$ -low staggering. The reversal of the staggering phase, induced by coupling to the quasiparticle degrees of freedom, appears to be a different mechanism than the spread of the collective wave function. It is evident from Table II that there is no correlation between the value of the triaxiality parameter  $\gamma$  of the mean-field and the staggering phase (see the Ru chain). The only visible trend is that for "axial" nuclei, which have a high-lying  $\gamma$  band,  $E(2_2^+)/E(2_1^+) \sim 10$ , the triaxiality parameter scatters around  $\gamma = 20^\circ$ , and for "triaxial" nuclei, which have a low-lying  $\gamma$  band  $E(2_2^+)/E(2_1^+) < 5$ , it scatters around  $\gamma = 30^\circ$ . This trend is expected when one interprets the  $\gamma$ -band as an anharmonic tidal wave, intermediating the harmonic and static limits (for discussion of tidal waves in weakly deformed nuclei, see Ref. [27]).

The question that naturally arises is what is the amount of the quasiparticle mixing in the even- $I$ -down case as com-

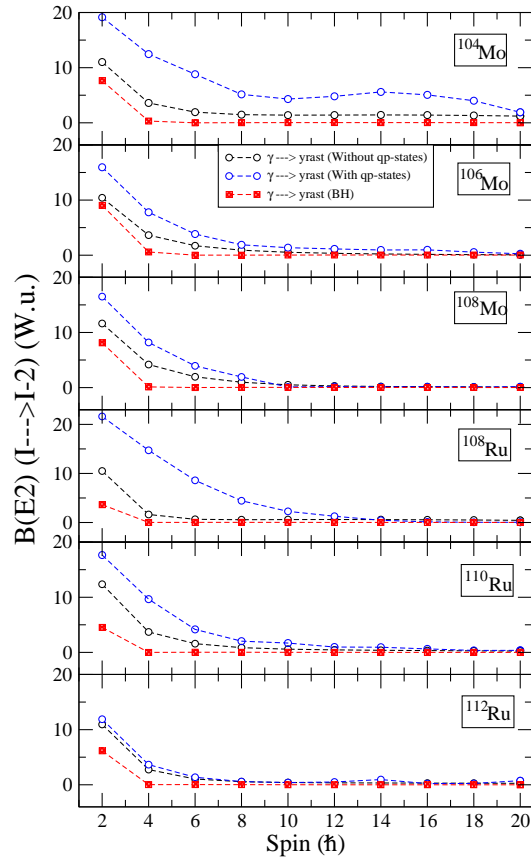


FIG. 9. (Color online) Reduced E2 probabilities for  $\Delta I = 2$  transitions from the  $\gamma$  band to the ground band. The blue and black circles show the TPSM values with and without coupling to the quasiparticle excitations, respectively. The red squares show the BH values.

pared to the odd- $I$ -down example. The mixing amplitudes are plotted in Figs. 6 for  $^{108}\text{Ru}$  and  $^{112}\text{Ru}$  as two examples belonging to former and latter cases, respectively. The amplitudes are shown separately for vacuum, two- and four-quasiparticle configurations. In  $^{108}\text{Ru}$ , both yrast and  $\gamma$  bands are dominated by the vacuum configuration up to  $I=8$  and above this spin value, the two-quasiparticle configurations dominate. This is due to the well established crossing of the two-quasiparticle aligned band with the ground-state band. For  $^{112}\text{Ru}$ , the only difference in comparison to  $^{108}\text{Ru}$  is that crossover occurs at  $I=10$  rather than at  $I=8$ . In particular, the magnitude of the two-quasiparticle admixture is very similar in the two nuclei. One would have expected that due to smaller contribution from quasiparticle excitations,  $^{112}\text{Ru}$  maintains the odd- $I$ -low staggering of the vacuum state. However, considering the similar quasiparticle admixtures for  $^{108}\text{Ru}$  and  $^{112}\text{Ru}$ , the reason for having different staggering phases in the two nuclei must be rooted in the nature of the quasineutron states at the Fermi level.

To further probe the dependence of the  $\gamma$ -band staggering

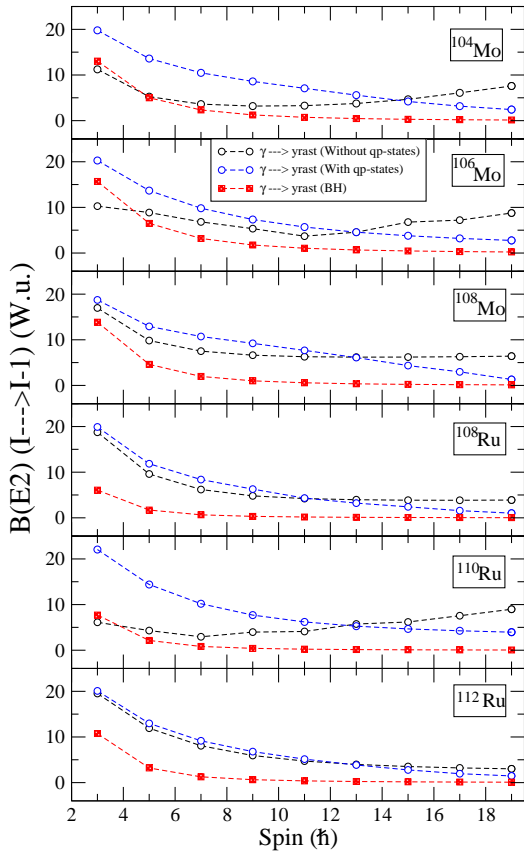


FIG. 10. (Color online) Reduced E2 probabilities for  $\Delta I = 1$  transitions from the  $\gamma$  band to the ground band. The blue and black circles show the TPSM values with and without coupling to the quasiparticle excitations, respectively. The red squares show the BH values.

on the magnitude of triaxiality, Fig. 7 displays  $S(I)$  for  $^{108}\text{Ru}$  and  $^{112}\text{Ru}$  with different values of  $\epsilon'$ . The phase of  $S(I)$  remains even-I-down, as seen at axial shape, for any value of  $\epsilon'$  chosen in  $^{108}\text{Ru}$ . On the other hand, in  $^{112}\text{Ru}$  the phase of  $S(I)$  changes sign with increasing triaxiality. In order to reproduce the observed phase for the  $\gamma$ -band, the triaxial deformation parameter of  $\epsilon' = 0.13$  ( $\gamma = 24^\circ$ ) is needed. This suggests that the quasineutron states at the Fermi level couple differently to the triaxial potential in the two cases.

### B. Comparison of the transitional probabilities : TPSM and Bohr Hamiltonian

In the framework of the collective model, even-I-down staggering pattern indicates a  $\gamma$ -soft potential energy surface of the Bohr Hamiltonian, and the odd-I-down suggests the presence of a substantial minimum at a finite  $\gamma$ -value [4, 8, 12]. As demonstrated in the preceding section, the TPSM reproduces the experimental  $S(I)$  values without any obvious relation to

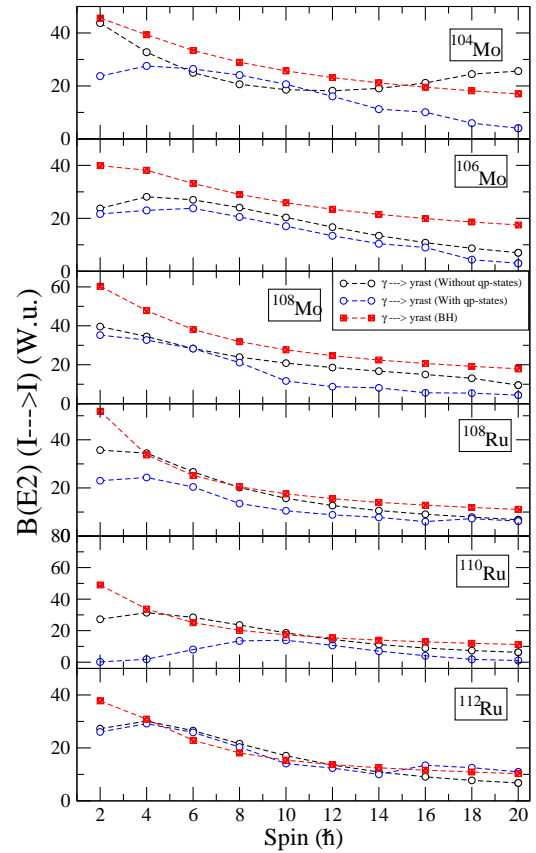


FIG. 11. (Color online) Reduced E2 probabilities for  $\Delta I = 0$  transitions from the  $\gamma$  band to the ground band. The blue and black circles show the TPSM values with and without coupling to the quasiparticle excitations, respectively. The red squares show the BH values. Except for  $^{112}\text{Ru}$  the values for the lowest spins are out of the frame.

$\gamma$ -softness. In an effort to elucidate the results obtained in the TPSM approach, we have also performed collective model calculations by adjusting its parameters to the TPSM transition energies. We employed a simplified version Bohr Hamiltonian (BH) of Ref. [8] that assumes irrotational-flow inertial parameters and a two-parameter potential energy of the form

$$\hat{H}_{GCM3} = \hat{\Lambda}^2 + \chi [1 - \cos 3\gamma + \xi \cos^2 3\gamma], \quad (15)$$

where  $\hat{\Lambda}^2$  is the O(6) part of the Bohr kinetic energy operator,  $\chi$  controls the softness and  $\xi$  the depth of the minimum at finite  $\gamma$ . The energy in units of  $E(2_1^+)$  depend only on  $\chi$  and  $\xi$ . The two parameters have been fixed by a least-squares-fit to the TPSM energies of the lowest members of the ground- and  $\gamma$ - bands. The standard quadrupole operator is used, and its scale is adjusted to the experimental value of  $B(E2, 2_1^+ \rightarrow 0_1^+)$ .

To compare the results obtained in the two approaches, we have chosen Ru- and Mo-isotopes as illustrative examples. The results for the other isotopic chains shall be presented in a separate detailed comparison of the two approaches [53].



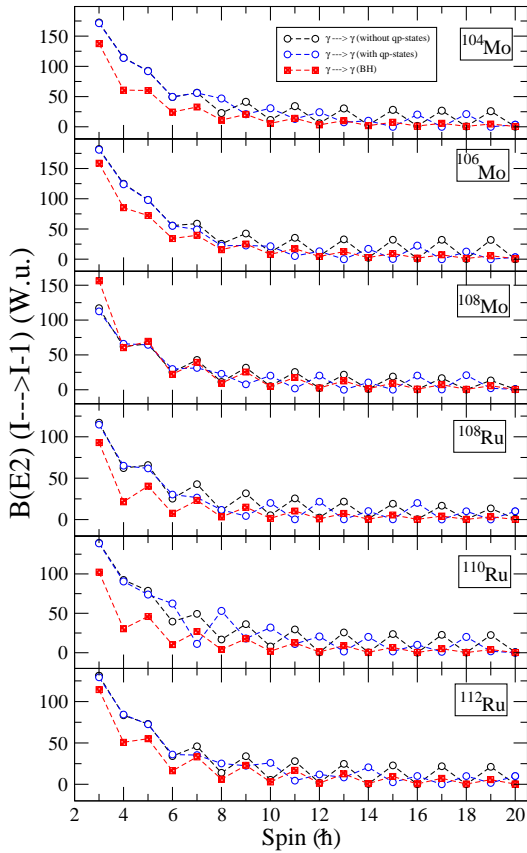


FIG. 12. (Color online) Reduced E2 probabilities for  $\Delta I = 1$  transitions between the  $\gamma$  band members. The blue and black circles show the TPSM values with and without coupling to the quasiparticle excitations, respectively. The red squares show the BH values.

In Fig. 8, the staggering parameter obtained in the two approaches is compared and it is evident from the figure that TPSM staggering is reasonably reproduced by the BH model. In order to further probe the two approaches, we have also evaluated the transition probabilities. Figs. 9 -13 depict the TPSM  $B(E2)$  values and compares them with the values obtained from the BH approach. Fig. 9 indicates that at low spin, the TPSM predicts large  $B(E2)$  values for the transitions  $I_\gamma \rightarrow (I-2)_g$  from the  $\gamma$  to the ground band, whereas according to the BH model only the transition  $2_2^+ \rightarrow 0_1^+$  is significantly large. All other transitions are practically quenched. At high spin, both models predict very small  $B(E2)$  for the transitions. The low-spin BH values for  $^{108,112}\text{Ru}$  are substantially smaller than the corresponding TPSM values.

Fig. 10 shows the transitions  $I_\gamma \rightarrow (I-1)_g$  from  $\gamma$ - to the ground-band. The  $B(E2)$  values for the  $3_1^+ \rightarrow 2_1^+$  are similar for both the models in the case of the Mo isotopes, but that the low-spin BH values for  $^{108,110}\text{Ru}$  are substantially smaller than the TPSM ones. Similar to the  $I_\gamma \rightarrow (I-2)_g$  transitions,  $B(E2, I_\gamma \rightarrow (I-1)_g)$  decrease more rapidly with “ $I$ ” for the

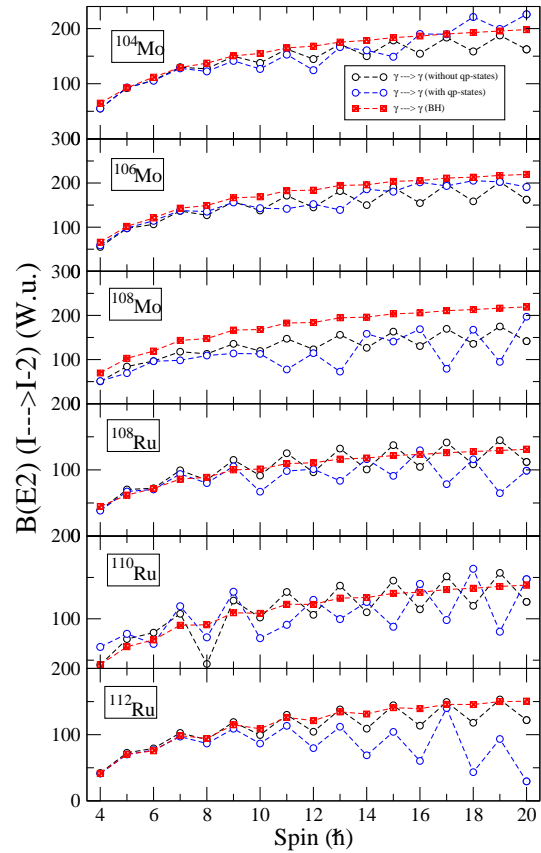


FIG. 13. (Color online) Reduced E2 probabilities for  $\Delta I = 2$  transitions between the  $\gamma$  band members. The blue and black circles show the TPSM values with and without coupling to the quasiparticle excitations, respectively. The red squares show the BH values.

BH and for the TPSM. TPSM calculations for  $B(M1)$  transition probabilities, shown in Fig. 14, indicate that transitions are almost pure E2. Fig. 11 shows that for the transitions  $I_\gamma \rightarrow I_g$  from the  $\gamma$ - to the ground-band, the  $B(E2)$  from BH are similar to the TPSM value without the quasiparticle admixture. Fig. 12 shows that for the transitions  $I_\gamma \rightarrow (I-1)_\gamma$  between the members of the  $\gamma$ -band, the BH values show the staggering pattern of the TPSM without the quasiparticle admixtures. The TPSM depicts the reversed pattern after the coupling to the quasiparticles is taken into account. At higher spins the BH values decrease more rapidly than the TPSM values. However, according to the TPSM calculations, shown in Fig. 15, the transitions are predominantly M1. It will be difficult to identify the differences in the staggering pattern, because the E2 part is of the order of 10-20 %.

The  $I$  dependence of the BH results can be qualitatively understood as follows. The kinetic part  $\hat{\Lambda}^2$  of the BH in Eq. 15 becomes dominant with increasing  $I$ . That is, it approaches the limit of the  $\gamma$ -independent Willets-Jean model. As discussed in detail in Ref. [54], the states are grouped into

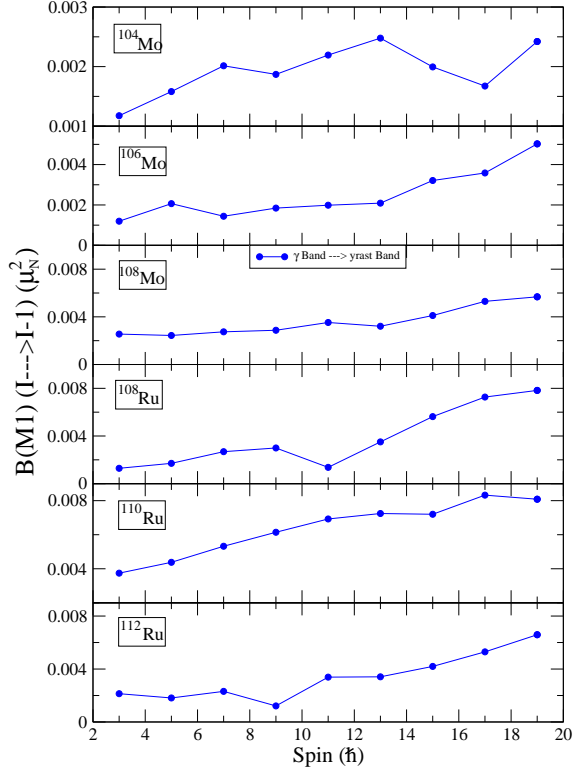


FIG. 14. (Color online) Reduced M1 probabilities for  $\Delta I = 1$  transitions from the  $\gamma$  band to the ground band.

SO(5) seniority multiplets ( $\nu=0,1,2,\dots$ ). [See, e.g., Fig. 1 of Ref. [54]. The reader can read the label "N" in that figure as if it were " $\nu$ ". There is a parity quantum number in  $R^5$ , which goes as  $(-1)^\nu$ . The quadrupole operator  $Q$ , which generates the  $E2$  transitions, carries  $\nu = 1$ , and thus negative  $R^5$  parity. Between the SO(5) triangularity and parity constraints, this means  $Q$  can only ladder  $\nu$  up or down by 1. This hardly is a surprise, since  $Q$  is the 5-dimensional quadrupole oscillator ladder operator, and the oscillator is a special case of SO(5) symmetry. In summary, the following selection rules act in the Willets-Jean limit:

$$\begin{aligned}
 I_\gamma \rightarrow (I-2)_g & \quad (I_\gamma \text{ even}) - \text{forbidden by } \Delta\nu=2 \\
 I_\gamma \rightarrow (I-1)_g & \quad (I_\gamma \text{ odd}) - \text{forbidden by } \Delta\nu=2 \\
 I_\gamma \rightarrow I_g & \quad (I_\gamma \text{ even}) - \text{allowed by } \Delta\nu=1 \\
 I_\gamma \rightarrow (I-1)_\gamma & \quad (I_\gamma \text{ even}) - \text{forbidden by } \Delta\nu=0 \\
 I_\gamma \rightarrow (I-1)_\gamma & \quad (I_\gamma \text{ odd}) - \text{allowed by } \Delta\nu=1
 \end{aligned}$$

The rapid decrease of the  $B(E2, I_\gamma \rightarrow (I-2)_g)$  in Fig. 9 and of the  $B(E2, I_\gamma \rightarrow (I-1)_g)$  in Fig. 10 reflects that they are forbidden in the Willets-Jean limit, which is being approached with increasing  $I$ . The  $B(E2, I_\gamma \rightarrow I_g)$  in Fig. 11 remain large because they are allowed in the Willets-Jean limit. The analog holds for the  $B(E2, I_\gamma \rightarrow (I-1)_\gamma)$  in Fig. 12, which generates the staggering pattern. The transitions from the states with  $I$  even are quenched because they are forbidden and the

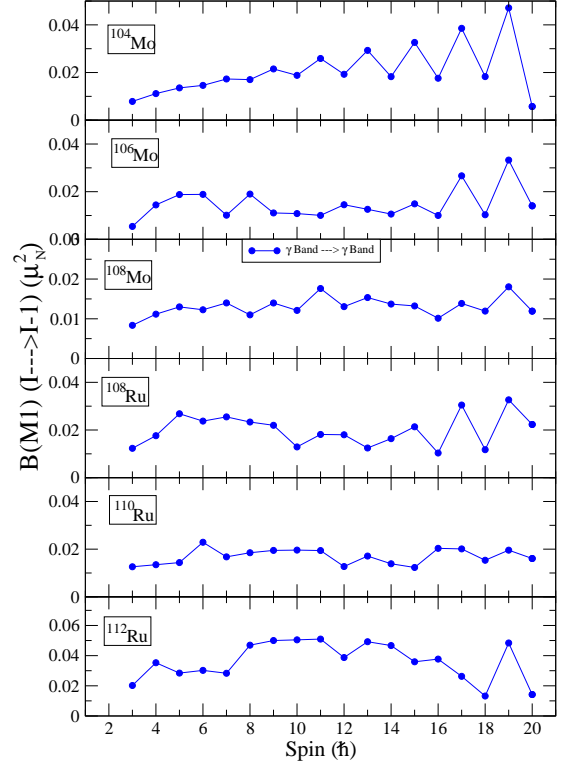


FIG. 15. (Color online) Reduced M1 probabilities for  $\Delta I = 1$  transitions between the  $\gamma$  band members.

transitions from odd  $I$  are not because they are allowed as per selection rules.

To differentiate the BH and TPSM models, it seem most promising to measure the  $B(E2, I_\gamma \rightarrow (I-2)_g)$  for  $I > 2$  and  $B(E2, I_\gamma \rightarrow (I-1)_g)$  for  $I > 3$ , which are much smaller for the BH than for the TPSM.

#### IV. CONCLUSIONS

In summary, a systematic investigation using the TPSM approach has been performed for nuclei in the Segré chart, where  $\gamma$ -bands, both for even- and odd-spin signatures, are known up to quite high spin. When only the vacuum configuration is taken into account, the  $\gamma$ -band staggering parameter,  $S(I)$  has always odd-I-down. It has been shown that for almost all the nuclei, the phase of  $S(I)$  changes from odd-I-down to even-I-down, when the quasiparticle excitations are taken into account in the configuration mixing framework. The only exceptions are the four nuclei of  $^{76}\text{Ge}$ ,  $^{112}\text{Ru}$ ,  $^{170}\text{Er}$  and  $^{232}\text{Th}$ . The staggering parameter calculated using the TPSM approach reproduces quite well the corresponding experimental values. In particular, the odd-I-down pattern, observed only in the aforementioned four nuclei nuclei, is reproduced in the TPSM approach.

The traditional interpretation of the collective model based on Bohr Hamiltonian, associates the even- $I$ -down pattern with a  $\gamma$ -soft shape and the odd- $I$ -down pattern with the presence of static triaxiality. In particular,  $^{76}\text{Ge}$  and  $^{112}\text{Ru}$  have been presented as rare examples of rigid triaxiality [12, 15, 28, 55]. In contrast, TPSM successfully accounts for the " $\gamma$ -soft" staggering pattern by assuming a rigid triaxial shape and explicitly considering the quasiparticle excitations that are expected to drive the system to the vibrational mode. However, it has been noted that the magnitude of the quasiparticle content in  $^{112}\text{Ru}$  ( $\gamma$ -rigid case) and  $^{108}\text{Ru}$  ( $\gamma$ -soft case) wavefunctions is similar. This suggests that the reason for staggering phase reversal obtained for all the studied nuclei, except for  $^{76}\text{Ge}$ ,  $^{112}\text{Ru}$ ,  $^{170}\text{Er}$  and  $^{232}\text{Th}$  is rooted in the nuclear shell structure.

To further examine the results obtained in the TPSM approach, we have also solved Bohr Hamiltonian. We studied staggering and  $B(E2)$  transition probabilities predicted by a two-parameter version of the Bohr Hamiltonian. The two parameters, which determine the softness and the presence of a minimum at finite " $\gamma$ " of the collective potential, were adjusted to the energies of the lowest members of the ground- and  $\gamma$ -bands as obtained in the TPSM approach. The fit re-

produces quite well the TPSM staggering pattern. However, there are significant differences between the reduced transition probabilities, which may allow one to delineate the two approaches. In particular, the Bohr Hamiltonian values of  $B(E2, I_\gamma \rightarrow (I-2)_g)$  and  $B(E2, I_\gamma \rightarrow (I-1)_g)$  for the transition from the " $\gamma$ " to the ground band fall off rapidly for  $I > 4(3)$ , whereas the TPSM values decrease much slower with  $I$ . The experimental data on transition probabilities is needed to shed light on the nature of the predicted transitions.

## V. ACKNOWLEDGEMENTS

The authors thank M. Caprio for illuminating discussions concerning the SO(5) selection rules. The work was partly supported by the US DoE grant DE-FG02-95-ER4093. Two of us (GHB and JAS) would like to acknowledge Department of Science and Technology, Govt. of India for providing financial support under Project no. CRG/2019/004960 to carry out a part of the research work.

- 
- [1] S. Frauendorf, Rev. Mod. Phys. **73**, 463 (2001).
  - [2] S. G. Nilsson, Dan. Mat. Fys. Medd. **29**, 16 (1955).
  - [3] A. Bohr and B. R. Mottelson, *Nuclear Structure*, Vol. II (Benjamin Inc., New York, 1975).
  - [4] N. V. Zamfir and R. F. Casten, Phys. Lett. **B 3**, 260 (1991).
  - [5] A. S. Davydov, in: Proc. Intern. Conf. on Nuclear structure (Kingston, Canada), eds. D. A. Bromley and E. W. Vogt (University of Toronto Press, Toronto, 1960) p. 801
  - [6] K. Kumar, Phys. Rev. **C 1**, 369 (1970).
  - [7] C. Baktash, J. X. Saladin, J. J. Ó'Brien, and J. G. Alassi, Phys. Rev. **C 18**, 131 (1978); **C 22**, 2383 (1980).
  - [8] M. Caprio, Phys. Rev. **C 83**, 064309 (2011).
  - [9] A. S. Davydov and G. P. Filippov, Nucl. Phys. **8**, 237 (1958).
  - [10] L. Wilets and M. Jean, Phys. Rev. **102**, 788 (1956).
  - [11] S. Frauendorf, Int. J. Mod. Phys. **E 38**, 1541001 (2015).
  - [12] E. A. McCutchan, Dennis Bonatsos, N. V. Zamfir and R. F. Casten, Phys. Rev. **C 76**, 024306 (2007).
  - [13] I. Stefanescu, A. Gelberg, J. Jolie, P. Van Isacker, P. von Brentano, Y.X. Luod, S.J. Zhu, J.O. Rasmussen, J.H. Hamilton, A.V. Ramayya, X.L. Che, Nucl. Phys. **A 789**, 125 (2007).
  - [14] J. A. Sheikh and K. Hara, Phys. Rev. Lett. **82**, 3968 (1999).
  - [15] G. H. Bhat, W. A. Dar, J. A. Sheikh, and Y. Sun, Phys. Rev. **C 89**, 014328 (2014).
  - [16] C. L. Zhang, G. H. Bhat, W. Nazarewicz, J. A. Sheikh, and Yue Shi, Phys. Rev. **C 92**, 034307 (2015).
  - [17] J. A. Sheikh, G. H. Bhat, Y. Sun, G. B. Vakil, and R. Palit, Phys. Rev. **C 77**, 034313 (2008).
  - [18] P. Ring and P. Schuck, *The Nuclear Many Body Problem* (Springer-Verlag, New York), (1980).
  - [19] Y. Sun, K. Hara, J. A. Sheikh, J. G. Hirsch, V. Velazquez, and M. Guidry, Phys. Rev. **C 61**, 064323 (2000).
  - [20] S. G. Nilsson, C. F. Tsang, A. Sobiczewski, Z. Szymanski, S. Wycech, C. Gustafson, I. Lamm, P. Moller, and B. Nilsson, Nucl. Phys. **A 131**, 1 (1969).
  - [21] Y. Sun and J.L. Egido, Nucl. Phys. **A 580**, 1 (1994).
  - [22] J. A. Sheikh, G. H. Bhat, Y.-X. Liu, F.-Q. Chen, and Y. Sun, Phys. Rev. **C 84**, 054314 (2011).
  - [23] G. H. Bhat, J. A. Sheikh, Y. Sun, and U. Garg, Phys. Rev. **C 86**, 047307 (2012).
  - [24] G. H. Bhat, J. A. Sheikh, and R. Palit, Phys. Lett. **B 707**, 250 (2012).
  - [25] S. Jehangir, G. H. Bhat, J. A. Sheikh, S. Frauendorf, S. N. T. Majola, P. A. Ganai, and J. F. Sharpey-Schafer, Phys. Rev. **C 97**, 014310 (2018).
  - [26] J. A. Sheikh, G. H. Bhat, W. A. Dar, S. Jehangir, and P. A. Ganai, Phys. Scr. **91**, 063015 (2016).
  - [27] S. Frauendorf, Y. Gu and J. Sun, Int. J. Mod. Phys. **E 20**, 465 (2011).
  - [28] Y. Toh, C. J. Chiara, E. A. McCutchan, W. B. Walters, R. V. F. Janssens, M. P. Carpenter, S. Zhu, R. Broda, B. Fornal, B. P. Kay, F. G. Kondev, W. Krölas, T. Lauritsen, C. J. Lister, T. Pawlat, D. Seweryniak, I. Stefanescu, N. J. Stone, J. Wrzesiński, K. Higashiyama, and N. Yoshinaga, Phys. Rev. **C 87**, 041304(R) (2013).
  - [29] A. D. Ayangeakaa R. V. F. Janssens, S. Zhu, D. Little, J. Henderson, C. Y. Wu, D. J. Hartley, M. Albers, K. Auranen, B. Bucher, M. P. Carpenter, P. Chowdhury, D. Cline, H. L. Crawford, P. Fallon, A. M. Forney, A. Gade, A. B. Hayes, F. G. Kondev, Krishichayan, T. Lauritsen, J. Li, A. O. Macchiavelli, D. Rhodes, D. Seweryniak, S. M. Stolze, W. B. Walters, and J. Wu, Phys. Rev. Lett. **123**, 102501 (2019).
  - [30] M. A. Lee, Nucl. Data Sheets, **31**, 381 (1980).
  - [31] H. Emling, E. Grosse, D. Schwalm, R. S. Simon, H. J. Wollersheim, D. Husar, and D. Pelte, Phys. Lett. **B 98**, 169 (1981).
  - [32] S. Raman, C. H. Malarkey, W. T. Milner, C. W. Nestor, Jr., and P. H. Stelson, Atom. Data Nucl. Data Tables **36**, 1 (1987).
  - [33] C. Y. Wu, D. Cline, M. W. Simon, R. Teng, K. Vetter, M. P. Carpenter, R. V. F. Janssens, and I. Wiedenhover, Phys. Rev. **C 61**, 021305 (2000).

- [34] C. Fahlander, A. Axelsson, M. Heinebrodt, T. Härtlein, and D. Schwalm, *Phys. Lett.* **B 388**, 475 (1996).
- [35] S. N. Majola, D. J. Hartley, L. L. Riedinger, J. F. Sharpey-Schafer, J. M. Allmond, C. Beausang, M. P. Carpenter, C. J. Chiara, N. Cooper, D. Curien, B. J. P. Gall, P. E. Garrett, R. V. F. Janssens, F. G. Kondev, W. D. Kulp, T. Lauritsen, E. A. McCutchan, D. Miller, J. Piot, N. Redon, M. A. Riley, J. Simpson, I. Stefanescu, V. Werner, X. Wang, J. L. Wood, C. H. Yu, and S. Zhu, *Phys. Rev.* **C 91**, 034330 (2015).
- [36] J. Simpson, P. A. Butler, P. D. Forsyth, J. F. Sharpey-Schafer, J. D. Garrett, G. B. Hagemann, B. Herskind, and L. P. Ekstrom, *J. Phys. G: Nucl. Phys.* **10**, 383 (1984).
- [37] A. Jungclaus, B. Binder, A. Dietrich, T. Härtlein, H. Bauer, Ch. Gund, D. Pansegrau, and D. Schwalm, *Phys. Rev.* **C 66**, 014312 (2002).
- [38] C. Y. Wu, D. Cline, M. W. Simon, G. A. Davis, and R. Teng, A. O. Macchiavelli, and K. Vetter, *Phys. Rev.* **C 64**, 064317 (2001).
- [39] A. Aprahamian, X. Wu, S. R. Leshner, D. D. Warner, W. Gulletly, H. G. Börner, F. Hoyler, K. Schreckenbach, R. F. Castene, Z. R. Shi, D. Kusnezov, M. Ibrahim, A. O. Macchiavelli, M. A. Brinkman, and J. A. Becker, *Nucl. Phys.* **A 764**, 42 (2006).
- [40] T. Härtlein, M. Heinebrodt, D. Schwalm, and C. Fahlander, *Eur. Phys. J. A* **2**, 253 (1998).
- [41] G. D. Dracoulis, G. J. Lane, F. G. Kondev, H. Watanabe, D. Seweryniak, S. Zhu, M. P. Carpenter, C. J. Chiara, R. V. F. Janssens, T. Lauritsen, C. J. Lister, E. A. McCutchan, and I. Stefanescu, *Phys. Rev.* **C 81**, 054313 (2010).
- [42] E. Ngijoi-Yogo, S. K. Tandel, G. Mukherjee, I. Shestakova, P. Chowdhury, C. Y. Wu, D. Cline, A. B. Hayes, R. Teng, R. M. Clark, P. Fallon, A. O. Macchiavelli, K. Vetter, F. G. Kondev, S. Langdown, P. M. Walker, C. Wheldon, and D. M. Cullen, *Phys. Rev.* **C 75**, 034305 (2007).
- [43] S. -C. Wu and H. Niu, *Nucl. Data Sheets* **100**, 483 (2003).
- [44] *Nucl. Data Sheets*, through Vol. **106**, (2005).
- [45] D. Ward, H. R. Andrews, G. C. Ball, A. Galindo-Uribarri, V. P. Janzen, T. Nakatsukasa, D. C. Radford, T. E. Drake, J. DeGraaf, S. Pilotte, and Y. R. Shimizu, *Nucl. Phys.* **A 600**, 88 (1996).
- [46] A. Guessous, N. Schulz, M. Bentale, E. Lubkiewicz, J.L. Durell, C.J. Pearson, W.R. Phillips, J.A. Shannon, W. Urban, B.J. Varley, I. Ahmad, C.J. Lister, L.R. Morss, K.L. Nash, C.W. Williams, S. Khazrouni, *Phys. Rev.* **C 53**, 1191 (1996).
- [47] H. Hua, C.Y. Wu, D. Cline, A.B. Hayes, R. Teng, R.M. Clark, P. Fallon, A. Goergen, A.O. Macchiavelli, K. Vetter, *Phys. Rev.* **C 69**, 014317 (2004).
- [48] L.M. Yang, S.-J. Zhu, K. Li, J.H. Hamilton, A.V. Ramayya, J.K. Hwang, X.Q. Zhang, L.Y. Zhu, C.-Y. Gan, M. Sakhaee, G.-L. Long, R.-Q. Xu, Z. Zhang, Z. Jiang, J. Myong-Gil, W.C. Ma, B.R.S. Babu, J. Komicki, E.F. Jones, J.D. Cole, R. Aryaeinejad, M.W. Drigert, I.Y. Lee, J.O. Rasmussen, M.A. Stoyer, G.M. Ter-Akopian, A.V. Daniel, *Chin. Phys. Lett.* **18**, 24 (2001).
- [49] X. L. Che, S. J. Zhu, J. H. Hamilton, A. V. Ramayya, J. K. Hwang, U. Yong-Nam, M. L. Li, R. C. Zheng, I. Y. Lee, J. O. Rasmussen, Y. X. Luo, W. C. Ma, *Chin. Phys. Lett.* **21**, 1904 (2004).
- [50] E. F. Jones, P. M. Gore, S. J. Zhu, J. H. Hamilton, A. V. Ramayya, J. K. Hwang, R. Q. Xu, L. M. Yang, K. Li, Z. Jiang, Z. Zhang, S. D. Xiao, X. Q. Zhang, W. C. Ma, J. D. Cole, M. W. Drigert, I. Y. Lee, J. O. Rasmussen, Y. X. Luo and M. A. Stoyer, *Phys. of Atomic Nuclei*, **69**, 7 (2006).
- [51] S. Rab, *Nucl. Data Sheets* **63**, 1 (1991).
- [52] A. R. Farhan and B. Singh, *Nucl. Data Sheets* **110**, 1917 (2009).
- [53] G. H. Bhat et al. (in preparation).
- [54] M. A. Caprio, D. J. Rowe, T. A. Welsh, *Comp. Phys. Com.* **180**, 1150 (2009).
- [55] D. T. Dohertya, J. M. Allmond, R. V. F. Janssens, W. Korten, S. Zhu, M. Zielińska, D. C. Radford, A. D. Ayangeakaa, B. Bucherd, J. C. Batchelder, C. W. Beausang, C. Campbell, M. P. Carpenter, D. Cline, H. L. Crawford, H. M. David, J. P. Delaroche, C. Dickerson, P. Fallon, A. Galindo-Uribarri, F. G. Kondev, J. L. Harker, A. B. Hayes, M. Hendricks, P. Humby, M. Girod, C. J. Gross, M. Klintefjord, K. Kolos, G. J. Lane, T. Lauritsen, J. Libert, A. O. Macchiavelli, P. J. Napiorkowski, E. Padilla-Rodal, R. C. Pardo, W. Reviol, D. G. Sarantites, G. Savard, D. Seweryniak, J. Srebrny, R. Varner, R. Vondrasek, A. Wiens, E. Wilson, J. L. Wood, C. Y. Wu, *Phys. Let.* **B 766**, 334 (2017).